Role of Water in the Multifaceted Catalytic Antibody 4B2 for Allylic Isomerization and Kemp Elimination Reactions

Orlando Acevedo*

Department of Chemistry and Biochemistry, Auburn University, Auburn, Alabama 36849

Received: July 21, 2009; Revised Manuscript Received: September 10, 2009

Specificity toward a single reaction is a well-known characteristic of catalytic antibodies. However, contrary to convention, catalytic antibody 4B2 possesses the ability to efficiently catalyze two unrelated reactions: a Kemp elimination and an allylic isomerization of a β,γ-unsaturated ketone. To elucidate how this multifaceted antibody operates, mixed quantum and molecular mechanics calculations coupled to Monte Carlo simulations were carried out. The antibody was determined to derive its adaptability for the mechanistically different reactions through the rearrangement of water molecules in the active site into advantageous geometric orientations for enhanced electrostatic stabilization. In the case of the Kemp elimination, a general base, Glu L34, carried out the proton abstraction from the isoxazole ring of 5-nitro-benzisoxazole while water molecules delivered specific stabilization at the transition state. The role of water was found to be more pronounced in the allylic isomerization because the solvent actively participated in the stepwise mechanism. A rate-limiting abstraction of the α-proton from the β,γ-unsaturated ketone via Glu L34 led to the formation of a neutral dienol intermediate, which was rapidly reprotonated at the γ-position via a solvent hydronium ion. Preferential channeling of H_3O^+ in the active site ensured a stereoselective proton exchange from the α- to the γ-position, in good agreement with deuterium exchange NMR and HPLC experiments. Ideas for improved water-mediated catalytic antibody designs are presented. In a technical advancement, improvements to a recent polynomial fitting and integration technique utilizing free energy perturbation theory delivered greater accuracy and speed gains.

Introduction

Multiple successful approaches have been taken in the development of catalysts for chemical reactions, ranging from small organic molecules[1] and transition metals[2] to the creation of designer proteins.[3,4] Catalytic antibodies are a particularly attractive option due to their ability to carry out complex stereospecific reactions in a benign environment; for example, aqueous solution at biological temperatures and pH.[5] A well-known caveat in the development of new antibody catalysts is that, due to their clonal nature, most antibodies are highly specific; that is, suited for only a single task. Hence, it was surprising to find that antibody 4B2 elicited from a cyclic amidinium salt (Scheme 1) originally intended to generate antibodies with glycosidase activity,[6] instead efficiently catalyzed a Kemp elimination ring-opening of 5-nitro-benzisoxazole ($k_{cat}/k_{uncat} = 18\,000$)[7] and an unrelated allylic rearrangement of a β,γ-unsaturated ketone ($k_{cat}/k_{uncat} = 1500$)[8] (Scheme 2). In addition, antibody 4B2's proficiency, $k_{cat}/(K_m/k_{uncat})$ of 1.2×10^6 M^{-1} for the allylic rearrangement[8] is higher than other reported antibodies designed for similar isomerization reactions.[9]

Antibody 4B2 is believed to utilize a glutamate residue (Glu L34) for proton abstraction in both reactions from a reported crystal structure which shows specific hydrogen bonding patterns with an analogous hapten (Scheme 1, R = H).[10] This general programmed base originated from the "bait-and-switch" method of using of a charged hapten to induce a complementarily charged amino acid in the binding site microenvironment.[11−13] Using haptens that do not precisely match the transition structure but instead elicit a strategically positioned functional residue has led to the development of other promiscuous antibodies capable of catalyzing multiple reactions with similar mechanisms.[7,9,14,15]

SCHEME 1: The Hapten Used to Elicit Antibody 4B2[a]

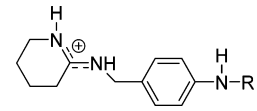

[a] R = CO−$(CH_2)_3$−CO−KLH.

The present study explores in detail the molecular fundamentals of antibody 4B2 in an effort to elucidate the reasons behind the significant rate enhancements reported for two very different reactions. A computational mechanistic investigation of the system has been carried out with particular emphasis on the active site residues and solvent molecules that play the largest roles in stabilizing the transition structures for the two reactions and determination of any similarities between the systems. Free energy profiles were obtained using mixed quantum and molecular mechanics (QM/MM) coupled to Monte Carlo (MC) simulations utilizing free energy perturbation (FEP) theory; a fifth-order polynomial quadrature method delivered a 7-fold increase in the speed of the calculations while retaining the accuracy of traditional potentials of mean force (PMF) methods.

Antibody 4B2 was found to catalyze both the Kemp elimination and the allylic isomerization reactions via the ionized Glu residue; however, the antibody was determined to derive its adaptability for the mechanistically different reactions through the inclusion of water molecules into its active site. The implications of a water-mediated active site are broad, as a recent study of theoretically designed and experimentally tested retro-

* E-mail: orlando.acevedo@auburn.edu.

10.1021/jp9069114 CCC: $40.75
Published on Web 10/27/2009

SCHEME 2: Antibody 4B2 Catalyzed (A) Kemp Elimination of 5-Nitro-benzisoxazole, and (B) Allylic Rearrangement of α-Cyclopent-1-en-1-yl-*p*-acetamidophenone (R = NHCOCH$_3$) via a Dienol or Dienolate Intermediate

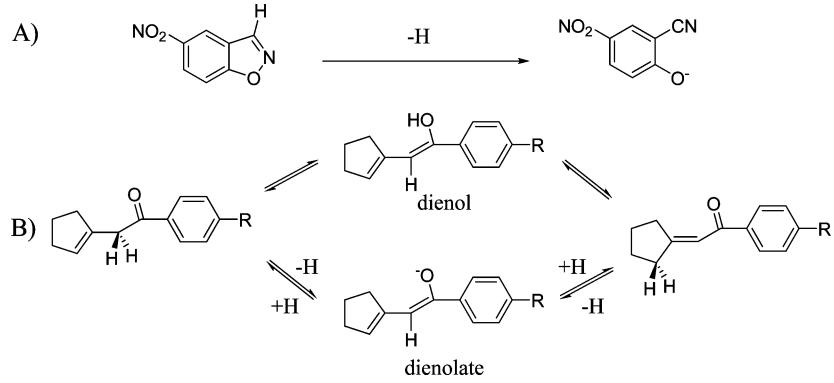

aldol enzymes found that the explicit inclusion of water molecules into the active site gave significant rate enhancements of up to 4 orders of magnitude greater than those that simply relied on charged side-chain networks.[3] Water plays a large role in the observed rate enhancements for antibody 4B2 by stabilizing developing charges at the transition state for both the elimination and isomerization reactions. In the case of the allylic rearrangement, water also mediates proton shuffling and ensures a stereoselective exchange. This study details changes for 4B2 along multiple reaction pathways for two considerably different reactions and allows for a better understanding of how the immediate molecular environment from solvent to protein affects the rate and selectivity of fundamentally important reactions. Greater insight into systematically constructing a multifaceted antibody useful for the catalysis of multiple organic reactions is presented.

Computational Methods

4B2 System. Mixed quantum and molecular mechanical (QM/MM) simulations were carried out to elucidate the specific interactions responsible for the enhanced reaction rates of a Kemp elimination and an allylic rearrangement delivered by antibody 4B2. The initial Cartesian coordinates for the antibody-ligand complex were derived from a reported 1.9-Å crystal structure of antibody 4B2 complexed with the cationic hapten shown in Scheme 1, where R = H.[10] The hapten was replaced with 5-nitro-benzisoxazole in the case of the Kemp elimination and α-cyclopent-1-en-1-yl-*p*-acetamidoacetophenone for the allylic rearrangement. The present model includes one active site and all 4B2 residues within 15 Å of it. Clipped residues were capped with acetyl or *N*-methylamine groups. The system was then subjected to conjugate-gradient energy minimization to relax the contacts between antibody residues and the substrate. The reduced 4B2 model consists of ∼2235 atoms and 129 residues out of 870 residues, which include the light and heavy chains of the antibody. The total charge of the system was set to zero by adjusting the protonation states of the residues furthest away from the center of the system. The entire system was solvated with a 22-Å cap containing 680−695 TIP4P[16] water molecules; a half-harmonic potential with a force constant of 1.5 kcal mol^{-1} Å^{-2} was applied to water molecules at a distance greater than 22 Å. As an example, the final model for the Kemp elimination is illustrated in Figure 1. To ensure that the final orientation of the water molecules within the enzyme binding pocket were not an artifact of the water cap, multiple reaction pathway simulations with different caps were carried out. The positions of the waters were determined to be conserved. In addition, geometric inspection of the water molecules resolved in the active site of antibody 4B2 from the reported crystal structure[10] was also consistent with the present simulations.

QM/MM Method. In our QM/MM implementation of the Kemp elimination, 5-nitro-benzisoxazole and the side chain Glu L34 were treated with the PDDG/PM3 semiempirical QM method.[17] PDDG/PM3 has been extensively tested for gas-phase structures and energetics[17,18] and has given excellent results for multiple condensed-phase QM/MM studies of organic and enzymatic reactions.[19−22] The remaining portion of the antibody was treated with MM atoms represented by the OPLS-AA force field[23] using residue-based cutoffs of 10 Å for all nonbonded interactions. "Capping" of the covalent bonds between the QM and MM parts of the system[24] and treatment of bonded interactions near the interface was handled using a movable link-atom approach[21] based on methodology originally developed by Guimarães et al.[25] In short, the QM system is capped with a hydrogen atom and placed coincident with the adjacent MM atom, and the partial charge from the link atom is added to the QM atom. This results in a charge distribution similar to that from the OPLS-AA force field. The appropriate MM terms are included in the potential energy function to avoid redundancies with the MM bond stretching, angle bending, and torsion terms. The link atoms are formally hydrogens, but in contrast to the standard link-atom formalism, their bonds to the QM region are elongated by ∼0.5 A to allow spatial coincidence. A link atom was placed on the α-carbon of Glu L34 residue. For the QM atomic charges, the CM3 charge model[26] was used with the charges scaled by 1.12 when the QM region had no net charge or unscaled for a net charge. The QM region of the simulation is composed of 26 total atoms for the Kemp elimination, including the link atom, which contains the substrate and part of Glu L34 (Figure 4B). A similar setup was used for the allylic rearrangement, which consisted primarily of Glu L34, the β,γ-unsaturated ketone, and a solvent hydronium ion. The QM region of the isomerization pathway was composed of 49 total atoms. In addition, several mechanisms were modeled in the rearrangement reaction, which necessitated the inclusion of multiple solvent molecules and the residue Tyr L96 into the QM region.

Reaction Coordinates. Potentials of mean force (PMF) calculations were used to build free-energy profiles for the reaction pathways of the elimination and rearrangement systems. In a PMF calculation, a reaction coordinate is driven using free-energy perturbations (FEP)[27] during Monte Carlo (MC) simulations. Experimental evidence suggests that both reactions are catalyzed via a proton abstraction involving Glu L34 acting as

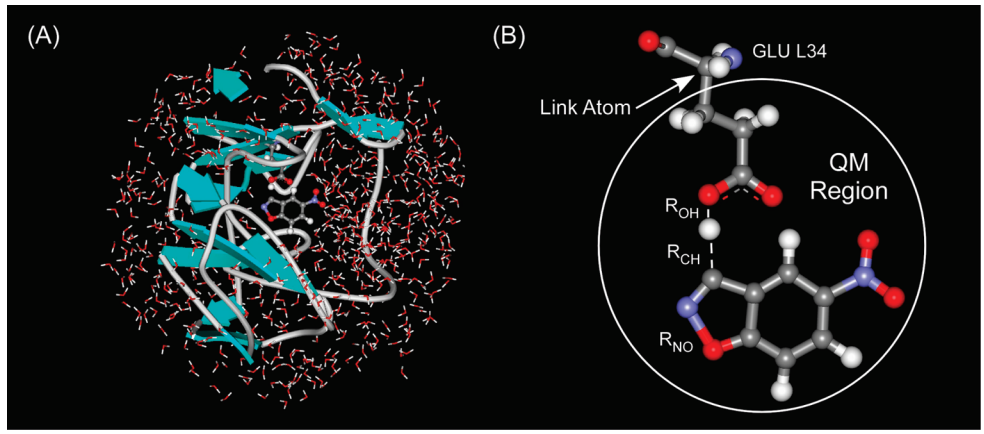

Figure 1. (A) Illustration of reduced antibody 4B2 consisting of 129 residues, 5-nitro-benzisoxazole with glutamate L34 (nearby waters removed for clarity), and a 22-Å water cap (coordinates from PDB ID: 1F3D[10]). (B) The QM region of the antibody active site consists of 25 atoms and 1 link atom. The reaction coordinates, $R_{OH} - R_{CH}$ and R_{NO}, were used to locate stationary points from free-energy maps obtained via PMF simulations. Illustrated structures correspond to the transition state computed from QM/MM calculations.

a general base.[8,10] Hence, the proton abstraction was computed in a series of "windows", each consisting of a small geometric perturbation; that is, stretching the bond. A common approximation for simultaneous bond making and breaking was used to reduce the dimensionality of the problem and is discussed in greater detail for the specific reactions below.[28]

Kemp Elimination. In the case involving the Kemp elimination, the reacting distance, $R_{OH} - R_{CH}$, is for the proton transfer between a Glu L34 oxygen and the hydrogen on the isoxazole ring, Figure 1B; $R_{OH} + R_{CH}$ is kept constant at 2.85 Å. The fixed distance of 2.85 Å was determined from gas-phase studies and Monte Carlo simulations of the substrate interacting with the active site. A second perturbation is necessary, R_{NO}, which entails the opening of the isoxazole ring via an increasing N−O distance. Combining the $R_{OH} - R_{CH}$ PMF that runs along one reaction coordinate with the R_{NO} PMF in a second direction produces a two-dimensional (2D) PMF. The result is a free-energy map that can be used to identify minima and the transition state present in the reaction. The breaking of the N−O bond was split into ∼30 windows with an increment of 0.04 Å; the resolution of the PMF is half of the window size (0.02 Å) due to the use of double-wide sampling.[29]

Allylic Rearrangemen. A similar simultaneous bond making and breaking coordinate for the proton transfer between Glu L34 and the α-hydrogen on α-cyclopent-1-en-1-yl-*p*-acetamidoacetophenone, $R_{OH} - R_{CH}$, was used in the first step of the allylic rearrangement leading to a dienolate intermediate with the $R_{OH} + R_{CH}$ distance kept constant at 2.85 Å. A dienol intermediate was also computed with two distinct possibilities for a concomitant addition of a hydrogen atom to the carbonyl oxygen while simultaneously abstracting the α-proton. The first attempt assumed the proton transfer occurring via a nearby solvent hydronium ion, and the second involved a proton shuffle occurring among the carbonyl oxygen, a water molecule, and Tyr L96. The addition of a proton to the γ-position of α-cyclopent-1-en-1-yl-*p*-acetamidoacetophenone was also modeled using a solvent hydronium ion, as predicted from experimental isotope labeling,[8] because no residues appeared close enough to deliver a proton. In all cases involving proton transfers with solvent, the simultaneous bond making and breaking distance was kept constant at 2.6 Å, which was found to be appropriate from gas phase calculations and our previous study on fatty acid amide hydrolase (FAAH).[21]

Fifth-Order Polynomial Method. For proton transfers, a novel method was developed in our previous work with FAAH, in which it was found that free-energy changes for individual windows can be fit almost perfectly by a cubic polynomial.[21] Using only 7 windows out of the usual 33 and analytically integrating the values yielded a quartic polynomial for the overall proton-transfer PMF that is essentially identical to running the full simulation. The largest deviation found between the approximate and the detailed calculation was 0.5 kcal/mol; the number of windows required for the PMF was reduced from approximately 900 to 65, with little loss of accuracy.[21] The cubic polynomial method does have drawbacks, most notably is a significant reduction in accuracy when computing elimination reactions (see Figure 2). To obtain more precise estimates of the current activation barriers, most of the proton transfer PMFs needed to be refined using every window, significantly reducing the efficiency of the calculations.

To overcome this limitation in the cubic polynomial methodology, the seven windows were fit instead with a fifth-order polynomial and analytically integrated to yield the full PMF. Energy values were considerably improved using the fifth-order polynomial method compared to our original cubic polynomial method. Higher-order polynomials were also tested, but were found to give nearly identical energies and polynomial fits ($\sim R^2 = 0.999$ to the seven windows) as compared to the fifth order. As an example, Figure 2 details two different proton transfers between 5-nitro-benzisoxazole and acetate acting as a base in a periodic box of 740 TIP4P water molecules, and 5-nitro-benzisoxazole in antibody 4B2 using the previously described methodology. In the case of acetate, the reaction coordinates mimic those of the 4B2 system with the exception that a $R_{OH} + R_{CH}$ constant value of 3.2 Å provided improved results. The fixed distance is consistent with a recent aqueous-phase QM/MM Kemp elimination study by Alexandrova et al. in which the chosen distance between 5-nitro-benzisoxazole and a free glutamate was also 3.2 Å.[30] In viewing Figure 2, with different fixed R_{NO} values as examples, it is immediately clear that a greater level of accuracy is obtained relative to the full 50 window "exact" PMF simulation when computing the free-energy profile using the fifth-order polynomial method, as compared to the cubic polynomial method. In addition, the computed $\Delta G^{\ddagger}$ of 25.6 kcal/mol for the Kemp elimination of 5-nitro-benzisoxazole by acetate in water is in good agreement with the experimentally measured value of 23.8 kcal/mol.[31] The new methodology provided a 7-fold improvement in speed over traditional PMF methods for the enzymatic calculations.

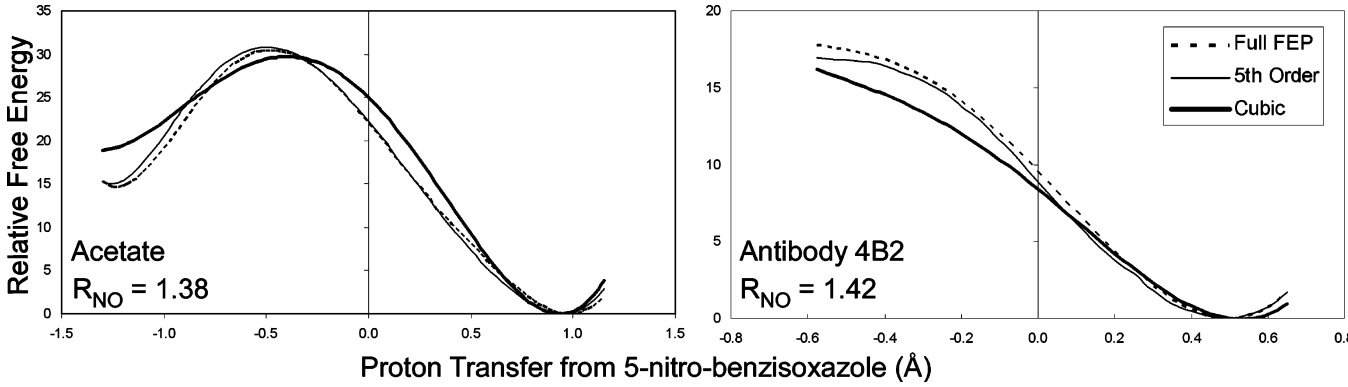

Figure 2. Proton transfers from 5-nitro-benzisoxazole to acetate (left) and antibody 4B2 (right) in water. The changes in ΔG (kcal/mol) are computed using the cubic and fifth-order polynomial methods, and the "exact" PMF, using 50 windows. All distances in Å.

Monte Carlo Simulation Protocol. All simulations were run at 25 °C using Metropolis Monte Carlo statistical mechanics. During the MC simulations, only the bond angles and dihedrals of side chains of residues with any atom within 10 Å of the center of the system are varied. All degrees of freedom in the QM region are varied, except the carbon atom adjacent to the link atom and those involved in the reaction coordinates, as previously discussed. Each simulation for a FEP window consists of 5×10^6 configurations of solvent relaxation, in which the water molecules were moved randomly while keeping the protein and substrate fixed, followed by 10×10^6 configurations of full equilibration for which all degrees of freedom are varied; and $25-50 \times 10^6$ configurations of averaging, in which all degrees of freedom were sampled and the free-energy changes were obtained. During the simulations, 10% of the attempted MC moves involve the active site, and 1%, the QM region. Each move of the QM region requires one self-consistent field QM calculation if the move is rejected and three if accepted (reference and two perturbed structures). Therefore, each FEP window requires $\sim(0.5-1) \times 10^6$ QM calculations; the total for this work exceeds 500×10^6, highlighting the importance of having very fast QM energy and charge evaluation, which the PDDG/PM3 model provides. All simulations were carried out using the program MCPRO.[32]

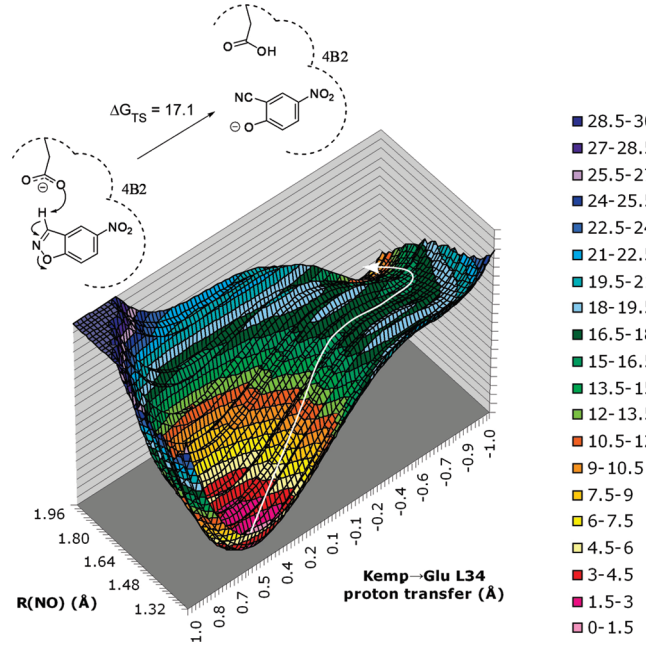

Figure 3. Free-energy profile (kcal/mol) for the Kemp elimination of 5-nitro-benzisoxazole in antibody 4B2. The reaction coordinate for the proton transfer is $R_{OH} - R_{CH}$ with $R_{OH} + R_{CH} = 2.85$ Å. Maximum free-energy values truncated to 30 kcal/mol for clarity.

Results and Discussion

Kemp Elimination in 4B2. The free-energy surface for the Kemp elimination of 5-nitro-benzisoxazole in antibody 4B2 via Glu L34 is shown in Figure 3. The reaction follows a concerted mechanism in which the R_{NO} distance of the isoxazole ring in the transition structure is 1.68 Å and the R_{OH} and R_{CH} distances are 1.20 and 1.65 Å, respectively. Changes in free energy were computed using our fifth-order polynomial fitting and analytical integration method and yielded a $\Delta G^{\ddagger}$ value of 17.1 kcal/mol. The level of uncertainty is less than ±1 kcal/mol on the basis of fluctuations in the averages for the individual FEP windows. To locate the critical points more precisely, the regions surrounding the reactants and transition state from the map were computed by using every FEP window. The $\Delta G^{\ddagger}$ from the "full" QM/MM/FEP simulation was 16.2 ± 1 kcal/mol. The experimental $\Delta G^{\ddagger}$ for the 4B2-catalyzed reaction is estimated at 19.7 kcal/mol from the reported conditions ($k_{cat} = 3.5 \pm 0.8 \times 10^2$ s^{-1}, pH 7.1, 1% CH_3CN, 40 mM phosphate buffer with 100 mM of NaCl, and 30 °C).[7] Although the predicted activation barrier is underestimated, the accuracy achieved is significantly better than recent QM/MM enzymatic simulations.[21,22,25,30,33]

Deviation from experimental values can often be attributed to systematic errors in computed energies when employing semiempirical methods in the QM/MM methodology.[20,25] However, for the Kemp elimination, the fifth-order polynomial methodology dramatically improved the accuracy of computed $\Delta G^{\ddagger}$ values compared to our earlier cubic polynomial quadrature method[21] using the same semiempirical method; that is, PDDG/PM3. For example, recent QM/MM calculations by Alexandrova et al.[30] employed the cubic polynomial method to study the ring-opening of 5-nitro-benzisoxazole as an essential part of the de novo design process in Baker's Kemp elimination enzymes.[4] The predicted PDDG/PM3 activation barriers were considerably underestimated as compared to experiment; for example, 8.1 ± 1 kcal/mol (exptl 20.0 kcal/mol) for KE07 and 12.3 ± 1 kcal/mol (exptl 19.8 kcal/mol) for KE15.[4,30] However, utilizing the fifth-order polynomial method for antibody 4B2, which is similar to the aforementioned enzymes, the energy was considerably improved, and the computational speed enhancement was retained.

To elucidate the origins behind 4B2's enzymatic activity, a good point of comparison is the Kemp elimination catalytic antibody 34E4.[14,33] Both antibodies employ a glutamate residue to deprotonate 5-nitro-benzisoxazole, and the activation barriers between 4B2 and 34E4 are reasonably similar, $\Delta G^{\ddagger}$ of 17.3 kcal/

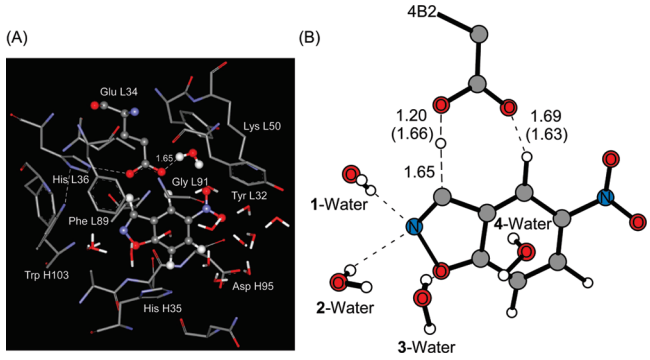

Figure 4. A representative snapshot of (A) 5-nitro-benzisoxazole in the active site of antibody 4B2 and (B) a close-up of the Kemp elimination transition structure with four nearby water molecules. Average distances over the final 25 million configurations for the transition state are given in angstroms (distances for ground state in parentheses).

mol ($k_{cat} = 0.66\ s^{-1}$, pH 7.4, 40 mM phosphate buffer with 100 mM of NaCl, and 30 °C).[31] However, the catalytic efficiency for the Kemp elimination in 34E4 is much more sensitive to the position of the substituent than antibody 4B2. For example, 5-NO_2 and 6-NO_2 substitutions on the benzisoxazole give k_{cat}/K_m values of 5450 and 0.177 $M^{-1}\ s^{-1}$, respectively, for 34E4 (20 °C, 40 nM phosphate, 100 nM NaCl, pH 7.4),[31] as compared to 39 and 6 $M^{-1}\ s^{-1}$ for 4B2 (30 °C, phosphate buffer pH 7.1, 0.5% CH_3CN).[7] Comparison of rate constants for the Kemp reaction catalyzed by a common base triethylamine, $k = 8.2 \times 10^{-1}$ and $1.6 \times 10^{-1}\ M^{-1}\ s^{-1}$ for 5-NO_2 and 6-NO_2,[34] respectively, suggests that the catalytic efficiency should be reasonably similar for the 6-NO_2-substituted benzisoxazole.[7] These observations led Tellier and co-workers to propose that transition state stabilization should change very little with nitro position substitution, particularly because 4B2 also delivered similar rates for the 5-NO_2- and 6-NO_2-substituted benzisoxazoles.[7]

Detailed insight on the active site changes along the reaction pathway is available from the present QM/MM/FEP calculations, which allows for the vicinity near the nitro position to be examined. A snapshot taken at the end of the Monte Carlo simulations near the transition state region, given in Figure 4, finds a number of hydrophobic and polar residues, and 13 water molecules within 5.0 Å of the 5-nitro-benzisoxazole. The nitro group of the substrate is primarily stabilized by water, and no steric demands are imposed in this region. The average distance over the final 25 million configurations of the simulation for the closest hydrogen of protonated Lys L50 to the nearest oxygen from the 5-NO_2 group was 3.74 Å; the average distances of the two closest ring-bound hydrogens from Tyr L32 were 2.51 and 2.71 Å to the nearest oxygens of the nitro group. Overall, the binding pocket is relatively loose, with the exception of the tight binding interactions between Glu L34 and the benzisoxazole (see Figure 4). This is in contrast to docking studies,[31] mutagenesis,[35] and crystal structures[12] of antibody 34E4, where a tight steric fit of the substrate within the active site is reported. The larger size of the 4B2 binding pocket allows for greater flexibility in accepting substrate substitutions not available to antibody 34E4, where the constricted enclosure influences substrate binding (K_m) to a considerable extent.[31]

A large active site could prove to be problematic in properly orienting the catalytic base for reaction. 4B2 overcomes this limitation through a strong hydrogen bond network present among the catalytic residue Glu L34, His L36, and Trp H103 that positions the base in the active site to deprotonate the 5-nitro-benzisoxazole and initiate ring-opening. Tight interacting distances of ~1.65 Å between the oxygens in Glu L34 and two ring-bound hydrogens on 5-nitro-benzisoxazole in the ground state anchor the substrate within the active site (see Figure 4B). In the case of the allylic isomerization reaction, the positioning of the carboxylate side chain allows the proton transfer to occur from the substrate stereoselectively (see Section 3.2, Allylic Isomerization in 4B2). This hydrogen bonding network was confirmed by the reported crystal structure of 4B2 with a bound hapten (Scheme 1, R = H)[10] and the present calculations detailing the reaction pathway (Figure 4A). From the simulations, His L36 points its hydrogen at the oxygen of Glu L34 at an average distance of 1.85 and 1.90 Å at the ground and transition states of the reaction pathway, respectively. The tautomeric form of His L36 is stabilized by Trp H103 via an average H-bond distance of 2.27 and 2.41 Å at the ground and transition states. The calculations agree with observations from the crystal structure, suggesting that the substrate cannot be deprotonated by His L36 because its unprotonated nitrogen atom points away from the reactant.

The ring-opening of 5-nitro-benzisoxazole (Scheme 2A) was determined by our calculations to be accelerated by a favorable aqueous microenvironment within the binding pocket in addition to proper alignment of the Glu L34 residue and the substrate. Four water molecules were found near the isoxazole ring throughout the entire reaction (see Figure 4). At the ground state, two of the water molecules help stabilize the substrate with average hydrogen bond distances of 2.14 and 2.21 Å from the N and O, respectively, to the nearest hydrogen of the **1**-water molecule and distances of 2.01 and 2.57 Å to N and O with the **2**-water molecule. Additional water molecules are found to interact with the NO_2 group, and an ordered water molecule was located near the Glu L34 residue with a HO−H···O−CO distance of ~1.65 Å at the ground state (see Figure 4A). The crystal structure of 4B2 bound with the amidinium hapten (Scheme 1, R = H) also finds a water molecule located adjacent to the Glu L34 residue.[10] Hydrogen bonding between a single water molecule and the anionic form of the base should have a significant effect on the rate acceleration delivered by the antibody. For example, a modest 10-fold increase in the base strength of a Glu carboxylate (ΔpK_a of 1.25) relative to an aqueous-phase carboxylic acid was reported for the 34E4 system whose crystal structure also showed an ordered water molecule near the base.[12] Hence, desolvation effects are unlikely to be the sole origin of enzyme activity in 4B2. A favorable electrostatic microenvironment for the transition state also contributes to the rate acceleration[36] as an additional water molecule complexes to the transition structure substrate (Figure 4B) when compared to the ground state. The average distances of N and O to the nearest aqueous H atom at the transition state were 2.08 and 3.65 Å for **1**-water, 2.37 and 2.65 Å for **2**-water, and 2.18 and 2.27 Å for **3**-water. In designing a multifaceted antibody, providing room in an otherwise hydrophobic binding pocket for a few water molecules to rearrange into advantageous geometric orientations allows for a flexible electrostatic microenvironment that can better stabilize the transition structure.

The Kemp ring-opening is extremely sensitive to small amounts of acetonitrile used to dissolve the substrate. Measured k_{cat}/K_m values in antibody 4B2 have been reported to be reduced by 90% in 10% acetonitrile and by 50% in 1% of the cosolvent.[7] Experimental $\Delta G^{\ddagger}$ values of 13.1 and 23.8 kcal/mol for the acetate-promoted elimination in acetonitrile and water, respectively,[31] suggest the observed rate reduction is not a bulk medium effect, but may be attributed to solvent sorting where

SCHEME 3: Newman Projections of α-Cyclopent-1-en-1-yl-*p*-acetamidoacetophenone

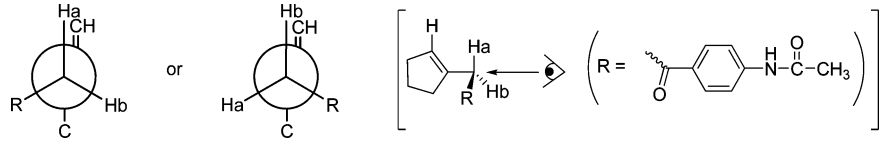

the hydrophobic binding site is preferentially occupied by acetonitrile.[7] To test this theory, QM/MM calculations were carried out with a single acetonitrile molecule placed in the QM region near the N and O atoms of the isoxazole ring of the substrate. The system was equilibrated for 70 million configurations of Monte Carlo sampling, and the entire free energy surface was recomputed in a fashion identical to the previous simulation. The refined transition structure geometry gave R_{OH} and R_{CH} distances of 1.22 and 1.63 Å, respectively, and a slightly lengthened R_{NO} distance of 1.72 Å as compared to the pure aqueous environment value of 1.68 Å. The inclusion of a single acetonitrile molecule raised the activation barrier by almost 2 kcal/mol with a $\Delta G^{\ddagger}$ value of 18.1 ± 1 kcal/mol compared to the original simulation value of 16.2 kcal/mol. The acetonitrile molecule resides in the pocket where the previous three water molecules (**1**-water, **2**-water, and **3**-water) were located, thereby disrupting the favorable hydrogen bond stabilization network (see Supporting Information Figure S1).

With the absence of a nearby general acid residue,[37] specific interactions with water molecules in the active site are crucial in stabilizing the emerging negative charge over the nitrogen and oxygen (−0.30 and −0.24 e CM3 charges, respectively) of the isoxazolyl breaking-bond in the transition state. The gas-phase reaction between 5-nitro-benzisoxazole and acetate at the B3LYP/6-31+G(d) theory level is consistent with the QM/MM/FEP results, with CHELPG[38] charges of −0.33 and −0.44 e on the nitrogen and oxygen transition state atoms, respectively.[31] In addition, a reduced gas-phase isoxazole model at the MP2/6-31+G(d)//HF/6-31G(d) theory level predicts a CHELPG charge of −0.34 e on the transition state oxygen and a 9.5 kcal/mol decrease in the activation barrier from the complexation of a single water molecule to the ring.[39]

Allylic Isomerization in 4B2. Several mechanisms for the allylic isomerization of α-cyclopent-1-en-1-yl-*p*-acetamidoacetophenone by antibody 4B2 were considered to clarify the sequence of proton transfer steps and whether the abstraction of the proton at the α-position or addition at the γ-position is rate-limiting. The system setup required careful consideration of the β,γ-unsaturated ketone positioning in the active site. The substrate, in a fashion similar to 5-nitro-benzisoxazole, was initially situated to maximize overlap with the bound hapten in the crystal structure.[10] However, the multiple rotatable bonds of the ketone compared to the benzisoxazole allowed for various conformations to potentially reside within the binding pocket. The conformational manifold for the ketone was extensively searched through a combination of manual docking and energy minimizations. Five different starting point poses were initially docked to minimize poor steric interactions with nearby side chains and were subsequently allowed to equilibrate for 135 million steps of QM/MM/Monte Carlo sampling, including all side chains within 10 Å of the ketone. As an example, Scheme 3 presents two different Newman projections along the view of the α-carbon adjacent to the carbonyl group, highlighting the two α-protons (H_a and H_b) available for abstraction. Both possibilities were docked into the active site and equilibrated prior to the chemical reaction. The final positioning of H_a for abstraction (left Newman projection in Scheme 3) gave a substantially lower energy configuration with favorable cation-π and electrostatic stabilization available from interactions between Lys L50 and the aromatic ring and adjacent carbonyl amide oxygen. The H_b-abstraction conformation unfavorably overlapped with residues and could not be positioned properly in the binding pocket. The same level of detail was given to the rotation of the carbonyl group adjacent to the abstracted proton to ensure the overall lowest energy conformer was chosen for simulation.

The mechanism of β,γ-unsaturated ketone isomerizations in most enzymes calls for a stepwise reaction with one of two possible intermediates present: a dienolate or dienol (Scheme 2B). The first path explored was the most straightforward with the abstraction of the α-proton by Glu L34 to yield a dienolate. A $\Delta G^{\ddagger}$ value of 20.5 kcal/mol was computed, and a ΔG of 20.4 kcal/mol for the intermediate was found relative to the reactants. The existence of the negatively charged dienolate was determined to be highly unstable in 4B2's active site designed to bind a positively charged hapten, and a reversible reaction is almost certain to occur prior to the protonation at the γ-position. From transition-state theory, free energies of activation for enzyme-catalyzed proton abstraction reactions range from ∼11 to 17 kcal/mol.[40,41] The computed $\Delta G^{\ddagger}$ is reasonable for the modest catalyst with a corresponding rate enhancement (k_{cat}/k_{uncat}) of 1500 ($k_{cat} = 1.6 \times 10^{-3}$ min^{-1}, pH 4.5, 50 mM of 10% (v/v) ethanol/acetate buffer, 150 mM NaCl, 30 °C).[8]

The second mechanistic possibility involves the formation of a neutral dienol intermediate. Measurements of pH dependence on the antibody-catalyzed reaction were reported to give a bell-shaped curve with maximum efficiency (k_{cat}/K_m) at ∼4.5 (optimal pH for the 4B2-Kemp elimination reaction was 7.5).[8] The curve could be indicative of a direct or indirect proton transfer from the protonated form of Glu L34 to the carbonyl oxygen of the substrate to yield the dienol. However, Glu L34's behaving exclusively as a general acid is inconsistent with the deprotonated form found in the crystal structure, which was crystallized at a pH value (pH = 5) close to the pH for optimal catalysis of the allylic isomerization (pH = 4.5 − 4.6).[10] This scenario would also leave open the question of the active base, although it could be possible that Glu L34 may act as a general acid at one point in the mechanism and a general base at another.

The pH curve may also suggest a second residue with a pK_a similar to that of Glu L34 behaving as a general acid and donating a proton in a concomitant fashion to the carbonyl oxygen during the α-proton abstraction. From the reported crystal structure,[10] however, there appears to be no residue capable of working in concert with Glu L34, and the modest rate acceleration observed in 4B2 is not consistent with that of a concerted allylic isomerization mechanism.[41] The present simulations did find Tyr L96 (pK_a = 10) to be within a reasonable distance of the substrate, ∼5.4 Å from the residue's side-chain oxygen to the ketone's carbonyl oxygen. A water molecule was found to lie between Tyr and the substrate. The calculation of a 2-D free energy map was attempted to quantify the possibility of an indirect proton transfer among Tyr L96, the water molecule, and the β,γ-unsaturated ketone. However, the Tyr residue was inappropriately positioned to

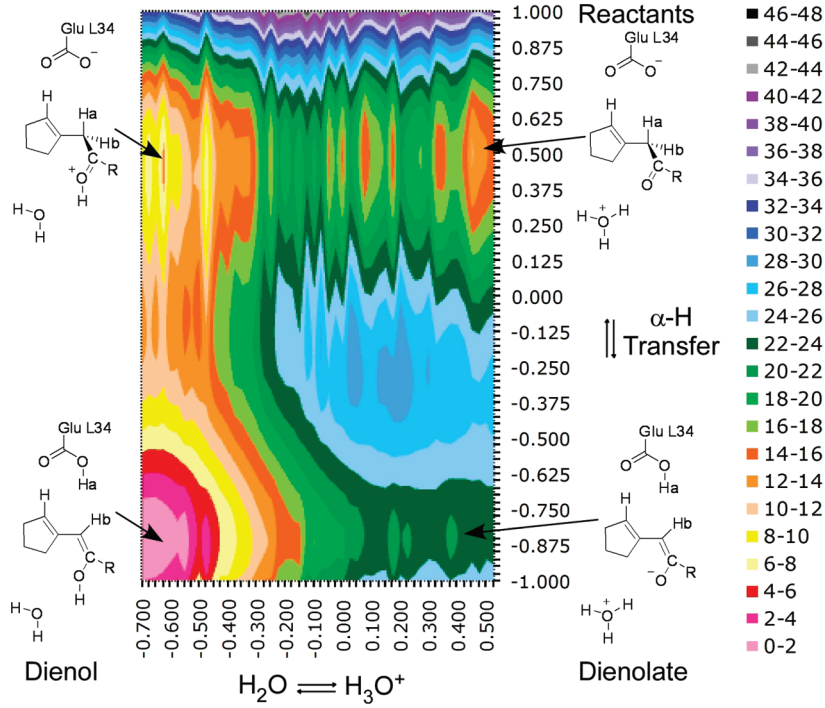

Figure 5. Computed two-dimensional free energy map (kcal/mol) for the α-proton abstraction catalyzed by antibody 4B2 in the presence of a hydronium solvent ion. All distances in Å; R = phenyl-NHCOCH$_3$.

donate its hydrogen atom in a synchronous fashion to the substrate, which led to convergence problems in the calculations.

An alternative interpretation of the pH bell-curve could imply that after behaving as a base, Glu L34 subsequently performs the function of an acid by protonating the γ-position in a stepwise fashion. This scenario has also been ruled out because HPLC monitoring of the isomerization reaction for the deuterated substrate in 4B2 found that the proton transfer from the α to the γ position is not direct.[8] However, a free solvent hydronium ion could provide the proper environment for dienol formation as deuterium exchange NMR experiments predict that H_3O^+ plays a substantial role in the mechanism, particularly in the addition of a proton at the γ-position.[8]

The necessity of a strong base and acid to occur simultaneously in the active site could explain the narrowness of the pH-dependent bell-shaped curve featuring a decline in k_{cat}/K_m below and above a pH of ~4.5.[8] To test this idea, a hydronium ion, which could have originated from the nearby Asp H95 residue or Glu L34 itself, was introduced near the carbonyl oxygen of the substrate in the binding pocket, and the system was allowed to equilibrate for 100 million QM/MM/Monte Carlo configurations. A free-energy surface for the α-proton abstraction was then computed using the fifth-order polynomial quadrature method following two simultaneous reaction coordinates: the α-proton abstraction from the β,γ-unsaturated ketone to the Glu L34 oxygen and the donation of a proton from the hydronium ion to the carbonyl oxygen. Figure 5 gives the free-energy surface with 2-D illustrations of representative stationary points. The presence of a H_3O^+ ion throughout the deprotonation gave a drop in the computed free-energy activation barrier to 12.6 kcal/mol, and the free energy of formation for the dienolate was also more favorable at 7.8 kcal/mol. A larger negative charge of −0.67 e for the carbonyl oxygen at the transition structure was computed with a H_3O^+ present, as compared to −0.53 e without the ion. Greater stabilization of the delocalized charge at the carbonyl oxygen via the hydronium ion allowed for an earlier transition state with R_{OH} and R_{CH} distances of 1.26 and 1.56 Å, respectively, as compared to 1.10 and 1.75 Å without the ion.

From the 2-D free energy map, the minimum energy path to the dienol intermediate is predicted to follow an initial protonation of the carbonyl oxygen via a hydronium ion, resulting in a positively charged substrate that is subsequently deprotonated at the α-carbon position. Refined calculations using every FEP window gave a $\Delta G^{\ddagger}$ of 9.4 kcal/mol for the ketone protonation and a ΔG of −1.6 kcal/mol for the resultant charged substrate relative to reactants. A relative activation barrier, $\Delta\Delta G^{\ddagger}$ of 2.3 kcal/mol for the Glu L34-mediated proton abstraction from the protonated substrate was computed. However, with the uncertainty in the calculations at approximately ±1 kcal/mol, the initial formation of a dienolate, $\Delta G^{\ddagger} = 12.6$ kcal/mol, followed by a subsequent protonation of the carbonyl oxygen to form the dienol, may also be competitive. Because no substantial activation barrier, <1 kcal/mol, was computed for the dienolate to dienol transformation, the predicted "stepwise" α-proton abstraction may appear "concerted" due to the short lifetime of the dienolate intermediate. Indeed, a measured substrate primary isotope effect of 2.2 on the kinetic constant (k_{cat}/K_m)[8] is far from the maximum possible value of 8−10 for a symmetrical transition state.[42] The transition state geometry for the α-proton abstraction of the protonated substrate was significantly more symmetrical, with computed R_{OH} and R_{CH} distances of 1.39 and 1.46 Å as compared to the more asymmetrical distances for the transition states, leading to a dienolate (Figure 6). Regardless of the initial proton abstraction pathway taken (Figure 7), both mechanisms predict the dienol to be the most favorable intermediate formed. A ΔG of −11.5 kcal/mol relative to the reactants was computed for the dienol as compared to the dienolate with ΔG values of 7.8 and 20.4 kcal/mol with and without the hydronium ion present, respectively.

The second half of the reaction mechanism incorporates a proton at the γ-position of the substrate to complete the isomerization. Kinetic measurements using deuterated substrates found that antibody 4B2 ensures a stereospecific exchange

A)

TS	R_{OH}	R_{CH}
dienolate	1.10	1.75
dienolate/H_3O^+	1.26	1.56
dienol	1.39	1.46

B)

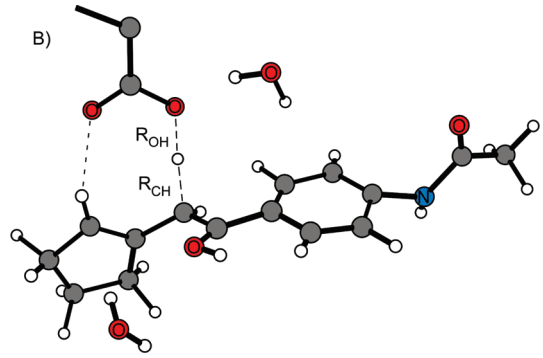

Figure 6. (A) Transition structure distances (Å) for R_{OH} and R_{CH} ($R_{OH} + R_{CH} = 2.85$ Å throughout the simulation) for the dienolate (with and without H_3O^+) and the dienol mechanisms in antibody 4B2 and (B) snapshot of the transition state for the protonated substrate leading to the dienol (two nearby water molecules are retained) from the QM/MM/FEP calculations.

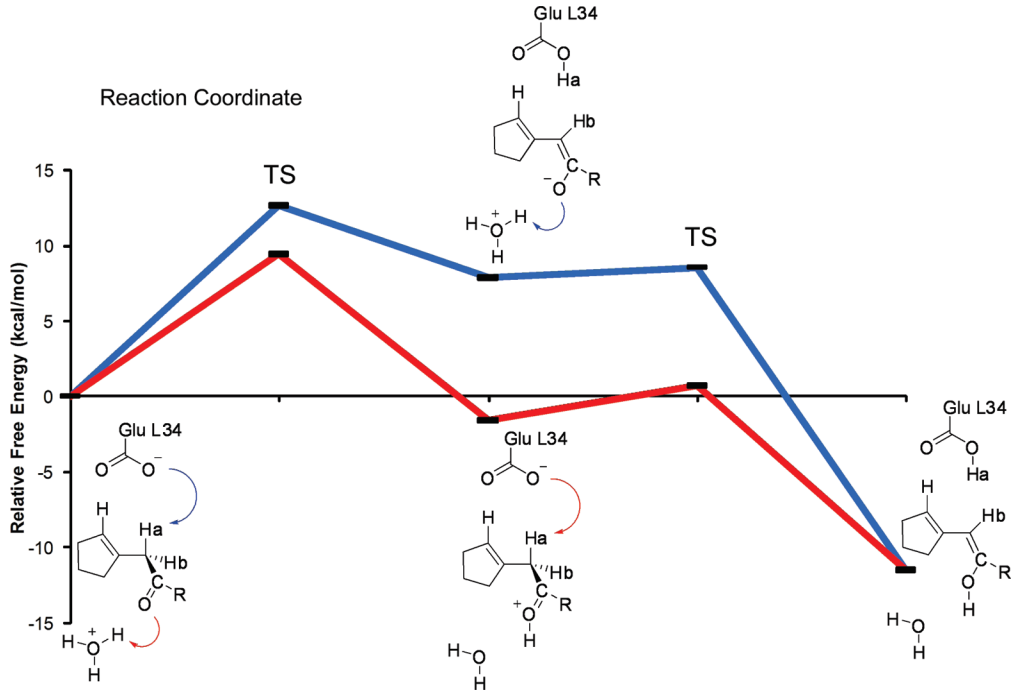

Figure 7. Competitive proton abstraction pathways toward dienol intermediate formation.

through the addition of a hydrogen to the same side of the face as the α-position abstraction.[8] The simulations find that preferential channeling of a solvent hydronium ion is responsible for the observed stereospecificity. From the calculations, the face opposite to the α-proton abstraction is blocked by Val H99 and H_3O^+ resides comfortably in a pocket formed between the dienol and residues His H35, Trp H47, Tyr L96, and Phe L89 (see Supporting Information Figure S2). Reprotonation at the γ-position of the dienol (and dienolate) intermediate was essentially spontaneous, with no discernible activation barrier computed for the transfer of a proton to the substrate when a hydronium ion is present (see Supporting Information Figures S3 and S4). To confirm the accuracy of the calculations, hysteresis error for the proton exchange between the hydronium solvent ion and the substrate at the γ-position was checked using the FEP simulations, and none was found (Figure S3).

Overall, from the simulations, the α-proton abstraction in the allylic isomerization is predicted to be catalyzed partially by desolvation effects on the Glu L34 base, similar to the Kemp elimination, and through a favorable microenvironment that allows a strong base and acid to occur simultaneously in the active site. Kinetic studies by NMR of the allylic isomerization find the initial α-proton abstraction should be reversible, but formation of the conjugated product is not.[8] Without the presence of a hydronium ion, the dienolate was determined to be highly unstable, ΔG of 20.4 kcal/mol, with a reversible reaction almost certain to occur before the protonation at the γ-position. With H_3O^+ present, a very shallow barrier allows for the rapid conversion of the dienolate to a dienol with a ΔG of −11.5 kcal/mol for the formation of the neutral intermediate from the reactants. The overall free energy of reaction, ΔG_{rxn}, of −26.7 kcal/mol for the conjugated product is significantly more difficult to revert back to reactants from either the charged or neutral intermediate, which is in line with experiment.

Conclusions

Computational mechanistic investigations for the Kemp elimination of 5-nitro-benzisoxazole and the allylic rearrangement of α-cyclopent-1-en-1-yl-*p*-acetamidoacetophenone by the catalytic antibody 4B2 were carried out. A general programmed base Glu L34 was found to be primarily responsible for the catalysis of both reactions. Proper positioning of the base in the binding pocket was controlled through a strong hydrogen bonding network between Glu L34 and nearby His and Trp residues. However, providing extra room in an otherwise

hydrophobic binding pocket for a few water molecules to rearrange into advantageous geometric orientations enabled a flexible microenvironment capable of catalyzing multiple reactions. In the case of the Kemp elimination, water molecules deliver specific stabilization through hydrogen bonding with the emerging negative charges over the isoxazolyl nitrogen and oxygen atoms at the transition state. The role of water was found to be more pronounced in the allylic isomerization, with the mechanism predicted to follow a stepwise path; the rate-limiting abstraction of the α-proton via Glu L34 leads to the formation of a neutral dienol intermediate that is rapidly reprotonated at the γ-position via a solvent hydronium ion. The H_3O^+ catalyzes the first step of the mechanism by stabilizing the large, developing, negative charge on the carbonyl oxygen prior to formation of the intermediate. In addition, preferential channeling of a H_3O^+ ion in the active site ensures a stereoselective proton exchange from the α- to the γ-position, in good agreement with observed deuterium exchange NMR and HPLC experiments and an extremely narrow pH-versus-k_{cat}/K_m efficiency range centered around a pH of 4.5.[8]

Significant effort has gone into improving rates for catalytic antibodies through reported attempts at increasing the basicity and positioning of the catalytic residue in the binding pocket.[11] In the case of the Kemp elimination, some success came from a bifunctional acid−base catalyst approach in which an antibody was elicited with an additional acidic residue in the active site to stabilize the emerging negative charge on the phenolate oxygen at the transition state.[13,37] However, precisely positioning side-chains is extremely difficult, and the present calculations suggest a reasonable alternative is to encourage water molecules to play the role of a general acid. Perhaps when designing a hapten, the inclusion of a specifically located bulky substituent could allow for the formation a small micropocket that water could fill when the reacting system is introduced. An additional advantage of including explicit waters into antibody design is increased flexibility, which in the case of antibody 4B2 contributes toward its ability to catalyze multiple reactions.

On the technical side, a fifth-order polynomial fitting and integration technique utilizing free energy perturbation theory was found to accurately reproduce free energy surfaces with a 7-fold increase in the speed of the calculations, as compared to traditional potentials of mean force methods. The methodological improvement should allow for more routine computational study of biological systems.

Acknowledgment. Gratitude is expressed to Auburn University for support of this research and to Dr. Ivan Tubert-Brohman for assistance.

Supporting Information Available: Snapshot of the Kemp elimination via antibody 4B2 in the transition state with a CH_3CN molecule present; dienol intermediate with H_3O^+ in the active site of antibody 4B2; free-energy profiles for proton exchange between H_3O^+ and dienolate/dienol intermediates at the γ-position. This material is available free of charge via the Internet at http://pubs.acs.org.

References and Notes

(1) Doyle, A. G.; Jacobsen, E. N. *Chem. Rev.* **2007**, *107*, 5713−5743.

(2) Leadbeater, N. E.; Marco, M. *Chem. Rev.* **2002**, *102*, 3217−3274.

(3) Jiang, L.; Althoff, E. A.; Clemente, F. R.; Doyle, L.; Röthlisberger, D.; Zanghellini, A.; Gallaher, J. L.; Betker, J. L.; Tanaka, F.; Barbas, C. F., III; Hilvert, D.; Houk, K. N.; Stoddard, B. L.; Baker, D. *Science* **2008**, *319*, 1387–1391.

(4) Röthlisberger, D.; Khersonsky, O.; Wollacott, A. M.; Jiang, L.; DeChancie, J.; Betker, J.; Gallaher, J. L.; Althoff, E. A.; Zanghellini, A.; Dym, O.; Albeck, S.; Houk, K. N.; Tawfik, D. S.; Baker, D. *Nature* **2008**, *453*, 190–195.

(5) (a) Tanaka, F. *Chem. Rev.* **2002**, *102*, 4885–4906. (b) Golinelli-Pimpaneau, B. *Curr. Opin. Struct. Biol.* **2000**, *10*, 697–708. (c) Karlstrom, A.; Zhong, G.; Rader, C.; Larsen, N. A.; Heine, A.; Fuller, R.; List, B.; Tanaka, F.; Wilson, I. A.; Barbas, C. F., III; Lerner, R. A. *Proc. Natl. Acad. Sci. U.S.A.* **2000**, *97*, 3878–3883. (d) Xu, J.; Deng, Q.; Chen, J.; Houk, K. N.; Bartek, J.; Hilvert, D.; Wilson, I. A. *Science* **1999**, *286*, 235–2348. (e) Heine, A.; Stura, E. A.; Yli-Kauhaluoma, J. T.; Gao, C.; Deng, Q.; Beno, B. R.; Houk, K. N.; Janda, K. D.; Wilson, I. A. *Science* **1998**, *279*, 1934–1940. (f) Romesberg, F. E.; Spiller, B.; Schultz, P. G.; Stevens, R. C. *Science* **1998**, *279*, 1929–1933. (g) Ulrich, H. D.; Mundorff, E.; Santarsiero, B. D.; Driggers, E. M.; Stevens, R. C.; Schultz, P. G. *Nature* **1997**, *389*, 271–274.

(6) Yu, J.; Hsieh, L. C.; Kochersperger, L.; Yonkovich, S.; Stephans, J. C.; Gallop, M. A.; Schultz, P. G. *Angew. Chem., Int. Ed.* **1994**, *33*, 339–341.

(7) Genre-Grandpierre, A.; Tellier, C.; Loirat, M.; Blanchard, D.; Hodgson, D. R. W.; Hollfelder, H.; Kirby, A. J. *Bioorg. Med. Chem. Lett.* **1997**, *7*, 2497–2502.

(8) Gonçalves, O.; Dintinger, T.; Lebreton, J.; Blanchard, D.; Tellier, C. *Biochem. J.* **2000**, *346*, 691–698.

(9) Lin, C. H.; Hoffmann, T. Z.; Wirsching, P.; Barbas, C. F., III; Janda, K. D.; Lerner, R. A. *Proc. Natl. Acad. Sci. U.S.A.* **1997**, *94*, 11773–11776.

(10) Golinelli-Pimpaneau, B.; Gonçalves, O.; Dintinger, T.; Blanchard, D.; Knossow, M.; Tellier, C. *Proc. Natl. Acad. Sci. U.S.A.* **2000**, *97*, 9892–9895.

(11) Xu, Y.; Yamamoto, N.; Janda, K. D. *Bioorg. Med. Chem.* **2004**, *12*, 5247–5268.

(12) Debler, E. W.; Ito, S.; Seebeck, F. P.; Heine, A.; Hilvert, D.; Wilson, I. A. *Proc. Natl. Acad. Sci. U.S.A.* **2005**, *102*, 4984–4989.

(13) Kikuchi, K.; Hannak, R. B.; Guo, M.-J.; Kirby, A. J.; Hilvert, D. *Bioorg. Med. Chem.* **2006**, *14*, 6189–6196.

(14) Thorn, S. N.; Daniels, R. G.; Auditor, M.-T. M.; Hilvert, D. *Nature* **1995**, *373*, 228–230.

(15) (a) Barbas, C. F., III; Heine, A.; Zhong, G.; Hoffmann, T.; Gramatikova, S.; Björnestedt, R.; List, B.; Anderson, J.; Stura, E. A.; Wilson, I. A.; Lerner, R. A. *Science* **1997**, *278*, 2085–2092. (b) Romesberg, F. E.; Flanagan, M. E.; Uno, T.; Schultz, P. G. *J. Am. Chem. Soc.* **1998**, *120*, 5160–5167. (c) Zheng, L.; Baumann, U.; Reymond, J.-L. *Proc. Natl. Acad. Sci. U.S.A.* **2004**, *101*, 3387–3392.

(16) Jorgensen, W. L.; Chandrasekhar, J.; Madura, J. D.; Impey, W.; Klein, M. L. *J. Chem. Phys.* **1983**, *79*, 926–935.

(17) Repasky, M. P.; Chandrasekhar, J.; Jorgensen, W. L. *J. Comput. Chem.* **2002**, *23*, 1601–1622.

(18) Sattelmeyer, K. W.; Tirado-Rives, J.; Jorgensen, W. L. *J. Phys. Chem. A* **2006**, *110*, 13551–13559.

(19) (a) Sheppard, A. N.; Acevedo, O. *J. Am. Chem. Soc.* **2009**, *131*, 2530–2540. (b) Sambasivarao, S. V.; Acevedo, O. *J. Chem. Theory Comput.* **2009**, *5*, 1038–1050. (c) Acevedo, O.; Squillacote, M. E. *J. Org. Chem.* **2008**, *73*, 912–922. (d) Acevedo, O.; Jorgensen, W. L. *J. Am. Chem. Soc.* **2006**, *128*, 6141–6146. (e) Acevedo, O.; Jorgensen, W. L. *J. Org. Chem.* **2006**, *71*, 4896–4902. (f) Acevedo, O.; Jorgensen, W. L. *J. Am. Chem. Soc.* **2005**, *127*, 8829–8834. (g) Acevedo, O.; Jorgensen, W. L. *Org. Lett.* **2004**, *6*, 2881–2884.

(20) (a) Acevedo, O.; Jorgensen, W. L.; Evanseck, J. D. *J. Chem. Theory Comput.* **2007**, *3*, 132–138. (b) Acevedo, O.; Jorgensen, W. L. *J. Chem. Theory Comput.* **2007**, *3*, 1412–1419.

(21) Tubert-Brohman, I.; Acevedo, O.; Jorgensen, W. L. *J. Am. Chem. Soc.* **2006**, *128*, 16904–16913.

(22) Acevedo, O.; Jorgensen, W. L. *Acc. Chem. Res.* **2009**, *42*, in press; http://dx.doi.org/10.1021/ar900171c.

(23) Jorgensen, W. L.; Maxwell, D. S.; Tirado-Rives, J. *J. Am. Chem. Soc.* **1996**, *118*, 11225–11236.

(24) (a) Singh, U. C.; Kollman, P. A. *J. Comput. Chem.* **1986**, *7*, 6663–6672. (b) Field, M. J.; Bash, P. A.; Karplus, M. *J. Comput. Chem.* **1990**, *11*, 700–733. (c) Eurenius, K. P.; Chatfield, D. C.; Brooks, B. R.; Hodoscek, M. *Int. J. Quantum Chem.* **1996**, *60*, 1189–1200. (d) Théry, V.; Rinaldi, D.; Rivail, J. L.; Maigret, B.; Ferenczy, G. G. *J. Comput. Chem.* **1994**, *15*, 269–282. (e) Monard, G.; Loos, M.; Théry, V.; Baka, K.; Rivail, J. L. *Int. J. Quantum Chem.* **1996**, *58*, 153–159. (f) Reuter, N.; Dejaegere, A.; Maigret, B.; Karplus, M. *J. Phys. Chem. A* **2000**, *104*, 1720–1735.

(25) Guimarães, C. R. W.; Udier-Blagovic, M.; Jorgensen, W. L. *J. Am. Chem. Soc.* **2005**, *127*, 3577–3588.

(26) Thompson, J. D.; Cramer, C. J.; Truhlar, D. G. *J. Comput. Chem.* **2003**, *24*, 1291–1304.

(27) Kollman, P. A. *Chem. Rev.* **1993**, *93*, 2395–2417.

(28) Gao, J.; Ma, S.; Major, D. T.; Nam, K.; Pu, J.; Truhlar, D. G. *Chem. Rev.* **2006**, *106*, 3188–3209.

(29) Jorgensen, W. L.; Ravimohan, C. *J. Chem. Phys.* **1985**, *83*, 3050–3054.

(30) Alexandrova, A. N.; Röthlisberger, D.; Baker, D.; Jorgensen, W. L. *J. Am. Chem. Soc.* **2008**, *130*, 15907–15915.
(31) Hu, Y.; Houk, K. N.; Kikuchi, K.; Hotta, K.; Hilvert, D. *J. Am. Chem. Soc.* **2004**, *126*, 8197–8205.
(32) Jorgensen, W. L.; Tirado-Rives, J. *J. Comput. Chem.* **2005**, *26*, 1689–1700.
(33) Alexandrova, A. N.; Jorgensen, W. L. *J. Phys. Chem. B* **2009**, *113*, 497–504.
(34) Kemp, D. S.; Cox, D. D.; Paul, K. G. *J. Am. Chem. Soc.* **1975**, *97*, 7312–7318.
(35) Seebeck, F. P.; Hilvert, D. *J. Am. Chem. Soc.* **2005**, *127*, 1307–1312.
(36) Warshel, A.; Sharma, P. K.; Kato, M.; Xiang, Y.; Liu, H.; Olsson, M. H. M. *Chem. Rev.* **2006**, *106*, 3210–3235.
(37) Müller, R.; Debler, E. W.; Steinmann, M.; Seebeck, F. P.; Wilson, I. A.; Hilvert, D. *J. Am. Chem. Soc.* **2007**, *129*, 460–461.
(38) Breneman, C. M.; Wiberg, K. B. *J. Comput. Chem.* **1990**, *11*, 361–373.
(39) Na, J.; Houk, K. N.; Hilvert, D. *J. Am. Chem. Soc.* **1996**, *118*, 6462–6471.
(40) Gerlt, J. A.; Gassman, P. G. *J. Am. Chem. Soc.* **1993**, *115*, 11552–11568.
(41) Hawkinson, D. C.; Eames, T. C. M.; Pollack, R. M. *Biochemistry* **1991**, *30*, 10849–10858.
(42) Westheimer, F. H. *Chem. Rev.* **1961**, *61*, 265–273.

JP9069114